Mathematical Model of a Gas Diffusion Electrode Bonded to a Polymer Electrolyte

Dawn M. Bernardi and Mark W. Verbrugge
Physical Chemistry Dept., General Motors Research Laboratories, Warren, MI 48090

A mathematical model for an ion-exchange membrane attached to a gas-fed porous electrode is derived and discussed. The model is applied to simulate the oxygen electrode of a polymer-electrolyte fuel cell. Our discussion focuses on cell polarization characteristics, water transport, and catalyst utilization—all of which must be considered for fuel-cell design. Calculated polarization behavior is shown to compare favorably with published experimental data. Our results indicate that if the membrane maintains full saturation, its contribution to the total cell resistance is most significant at higher operating current densities (greater than 200 mA/cm^2). Polarization resistance due to the oxygen reduction reaction appears to be important for all practical current densities. Water transport, driven by pressure and electric-potential forces, is shown to be a complicated function of the cell operating conditions. The utilization and distribution of noble-metal catalyst is discussed.

Introduction

It has been projected that in the not too distant future, the world population will double its current value and the global consumption of energy will have increased by a factor of five (Lindström, 1988). Such predictions offer motivation for the development of efficient power generators. In addition, it is desirable to design our future power systems so that only benign waste products are generated, modular construction is afforded, and quiet operation is observed. The recent development of perfluorosulfonic-acid (PSA) polymer-electrolyte fuel cells (McElroy and Nuttall, 1982; Nuttall and McElroy, 1983; Watkins, 1988; Ticianelli et al., 1988a,b) presents a promising approach to addressing our expanding energy requirements for stationary and vehicular applications. [The polymer electrolyte in these fuel cells is also referred to as an ion-exchange membrane (IEM), a proton-exchange membrane (PEM), or a solid polymer electrolyte.]

The premier advantage associated with fuel cells is that they are not limited by Carnot efficiency. No gases are heated to create explosive reactants, and no moving parts similar to pistons and crankshafts are required to convert thermal energy into mechanical energy. The energy released from the interatomic bonds of the reactants is converted more efficiently into usable electrical energy relative to traditional power-generating devices. Because no mobile electrolyte is employed, corrosion problems in the polymer-electrolyte fuel cell are reduced and cell construction is simplified. Operation of polymer-electrolyte cells, however, is complicated by the electro-osmotic flow of water through the PSA membrane pores—the conductivity of the membrane depends strongly on its water content, and during cell operation the membrane can become dehydrated, leading to a prohibitively resistive electrolyte and cell failure (Rieke et al., 1987). Once the heat, mass, and momentum transport characteristics are known, it should be possible to optimize the cell construction and operation as has been done for previous fuel-cell systems (Van Winkle and Carson, 1963; Newman, 1979).

It is the purpose of this study to develop the mathematical framework necessary to simulate a fuel-cell electrode bonded onto a membrane, a first step toward the development of a complete fuel-cell model. This is the first membrane-electrode model to include electro-osmotic convection, which, as alluded to above, is of critical importance to cell operation.

Recent work and references to past work on gas-diffusion-electrode and membrane-electrode models can be found in the articles by Björnbom (1986, 1987), Savinell and Fritts (1988), Fritts and Savinell (1989), Yang et al. (1989), Ridge et al. (1989), Viitanen and Lampinen (1990), and Giordano et al. (1991). In addition, the earlier series of articles by Burshtein et al. (1971, 1972) and by Chirkov et al. (1975a,b) are helpful particularly in classifying the different model approaches for

Correspondence concerning this article should be addressed to D. M. Bernardi.

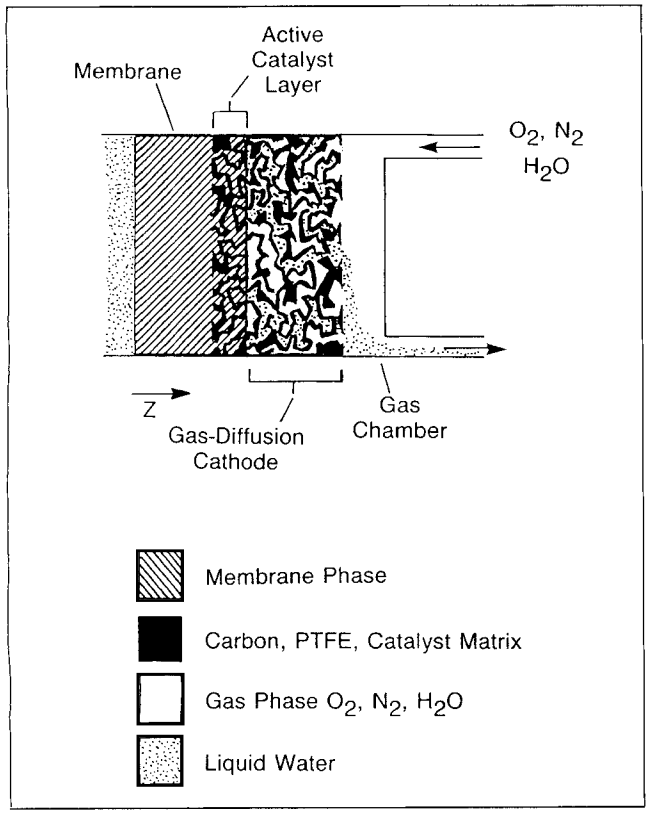

Figure 1. Gas diffusion electrode bonded to a solid polymer electrolyte.

porous gas diffusion electrodes and presenting comparisons between results of experiment and theory. The primary distinguishing difference between these studies and our work is the inclusion of electro-osmotic and pressure-driven water transport consonant with a polymer-electrolyte fuel cell.

We employ the gas-phase transport (Bernardi, 1990) and membrane (Verbrugge and Hill, 1990a) models previously developed in this laboratory to simulate the membrane/electrode system. In addition, we modify traditional porous-electrode theory (Tiedemann and Newman, 1975) to address the region where the membrane phase and electrode overlap, which we refer to as the active catalyst layer. The model, therefore, treats three distinct regions. Another unique feature of this work is that we simulate the system with only solid electrolyte (as opposed to both solid and liquid electrolytes) and therefore are able to compare our predicted polarization behavior to experimental results of polymer-electrolyte fuel cells with nearly reversible hydrogen electrodes (Ticianelli et al., 1988a,b). We do not address the fundamental interactions of gas bubbles with poly(tetrafluoroethylene) (PTFE) surfaces within the electrodes. Information regarding this can be found in the work of Jańczuk and Bialopiotrowicz (1989) and references therein.

For the present study, we restrict our attention to the oxygen electrode, which has been the subject of numerous studies (Holze and Vielstich, 1984) and is the limiting electrode (compared to the relatively efficient hydrogen electrode) of polymer-electrolyte fuel cells.

We first describe the membrane-electrode model mathematically, and then the model results are analyzed and compared with experimental data.

Mathematical Model

A membrane bonded to a gas diffusion electrode is shown in Figure 1. The gas diffusion electrode is composed of electronically-conductive material that has been made substantially hydrophobic by the addition of PTFE. The system is considered to be composed of three regions: a *membrane region* of hydrated PSA polymer electrolyte, an *active catalyst layer*, which is formed by the overlap of the membrane and the gas diffusion electrode, and a region termed the *gas diffuser*. The portion of the gas diffusion electrode that does not contain membrane, which we call the gas diffuser, provides three types of avenues for species transport:

1. Electrons move through the electronically-conductive portion consisting of carbon and catalyst (represented by the blackened area of the gas diffusion electrode in Figure 1).
2. Gaseous species (clear area) move through open pores wet-proofed by PTFE.
3. Liquid water (stippled portion) flows through channels that are not lined with PTFE.

The active catalyst layer is a very thin region, in which dissolved gaseous reactants can contact ions supplied by the membrane and electrochemical reaction can occur at the catalyst sites (e.g., Pt clusters). In the active catalyst layer, the membrane phase is depicted as penetrating the wet-proofed pores as well as pores that are not lined by PTFE. (In reality, a fraction of these pores may not be filled with membrane phase, and the boundary is diffuse and not sharp as shown in the illustration.) A gas chamber, which is adjacent to the gas diffuser, supplies and exhausts gas-phase reactants and liquid water. A reservoir of liquid water is depicted on the left in Figure 1, indicating that the membrane is always fully hydrated in this study.

Figure 1 illustrates the case of an air electrode, which we focus on throughout this investigation. For the air electrode, the reactant O_2 supplied at the gas chamber transports through the porous gas diffuser and dissolves into the polymer-electrolyte phase of the active catalyst layer. Protons in the membrane pores can react with dissolved O_2 at catalyst sites in the active layer to produce water in the overall electrochemical reaction. (Electrons for oxygen reduction are supplied to the electrode through a circuit connected to the counterelectrode, which is located at the membrane-reservoir interface and is not shown in Figure 1.)

$$O_2 + 4H^+ + 4e^- \rightleftharpoons 2H_2O. \qquad (I)$$

The direction of water flow through the system will depend on the relative magnitudes of electro-osmotic forces and pressure forces, both of which are incorporated into the model formulation. The protons in the pore water of the membrane are counterions, with positive charge that balances the negative charge associated with the fixed charge sites attached to the polymer backbone. The pore water is thus positively charged and will tend to be forced toward the electrode—down the membrane potential gradient.

The entire system, including the inlet reactant streams, is taken to be held at constant temperature, and the gases are assumed to be ideal. Since the gas-phase viscosity is quite small relative to the liquid phase, the total gas pressure within the gas diffuser is taken to be constant. The gases in the chamber are treated as well mixed, and therefore are of uniform composition. For the present study, we consider conditions, in

Table 1. Governing Equations for Fuel-Cell Membrane-Electrode Model

Membrane	Catalyst Layer	Gas Diffuser
$i = -I$	$\frac{di}{dz} = ai_0\{\exp[(\alpha_a f(\phi_{solid} - \phi)] - \exp[-\alpha_c f(\phi_{solid} - \phi)]\}$	—
—	$\sigma_c^{eff}\frac{d\phi_{solid}}{dz} = I + i$	$\sigma_d^{eff}\frac{d\phi_{solid}}{dz} = I$
$-\kappa\frac{d\phi}{dz} = i - Fc_f v$	$-\kappa^{eff}\frac{d\phi}{dz} = i - Fc_f v$	—
$\frac{dv}{dz} = 0$	$\rho\frac{dv_s}{dz} = -\frac{s_w}{nF}\frac{di}{dz}$	$\rho\frac{dv_s}{dz} = -\frac{dN_{w,g}}{dz}$
—	—	$\frac{p_L}{RT}\frac{D_{w-N_2}^{eff}}{x_{N_2}}\frac{dx_{N_2}}{dz} = \frac{I}{4F}r_{N_2} + N_{w,g}$
$\mathfrak{D}_{O_2}\frac{d^2c_{O_2}}{dz^2} = v\frac{dc_{O_2}}{dz}$	$\mathfrak{D}_{O_2}^{eff}\frac{d^2c_{O_2}}{dz^2} = v\frac{dc_{O_2}}{dz} + \frac{di}{dz}\left(\frac{s_{O_2}}{nF} - \frac{s_w}{nF}\frac{c_{O_2}}{\rho}\right)$	—
where	where	where
$v = \frac{k_\Phi}{\mu}z_f c_f F\frac{d\phi}{dz} - \frac{k_P}{\mu}\frac{dP}{dz}$	$v = \frac{k_\Phi^{eff}}{\mu}z_f c_f F\frac{d\phi}{dz} - \frac{k_P^{eff}}{\mu}\frac{dp}{dz}$	$v_s = -\frac{k_{P,s}^d}{\mu}\frac{dp}{dz}$
	$i_0 = i_0^{ref}\left(\frac{c_{O_2}}{c_{O_2}^{ref}}\right)^{\gamma_{O_2}}\left(\frac{c_{H^+}}{c_{H^+}^{ref}}\right)^{\gamma_{H^+}}$	$N_{w,g} = \frac{I}{4F}x_w^{sat}\left[1 - x_w^{sat} - x_{N_2} + \frac{x_{N_2}}{r_w}\right]^{-1}$

which water is available from either the membrane side or the chamber side of the system: we only consider the case of a fully-hydrated membrane and wetted liquid pores in the gas diffuser. Throughout the gas diffuser, the gas phase is taken to be in equilibrium with the liquid-water phase; hence, the gas-phase concentration of water, expressed as a mole fraction, is:

$$x_w^{sat} = \frac{p_w^{sat}}{p}. \tag{1}$$

Since the membrane and electrode are quite thin relative to the cell width, a one-dimensional macrohomogeneous description is appropriate. The equations developed in the following sections are summarized in Table 1. Six principal model equations are balanced by the following six variables: c_{O_2}, i, p, x_{N_2}, ϕ, and ϕ_{solid}. The model employs the following four phenomenological equations:

1. Nernst-Planck equation for ionic transport (Eq. 2)
2. modified form of Schlögl's velocity equation (Eq. 7)
3. Butler-Volmer relation (Eq. 15)
4. Stefan-Maxwell equation for gas-phase transport (Eq. 22).

The model is developed by combining these equations along with conservation of mass and energy in accordance with the laws of classical physics.

In general, properties of the active catalyst layer are designated by subscript c; those of the gas-diffuser region are denoted by subscript d; and unsubscripted quantities refer to membrane properties. Symbols D and $\mathfrak{D}$ are used for gas-phase diffusion coefficients and membrane-phase diffusion coefficients, respectively. Also, gas-phase and membrane-phase compositions of species i are expressed as mole fraction x_i and concentration c_i, respectively; concentrations c_i are based on the total membrane volume.

In the following subsections, we derive the equations consonant with the different regions of the membrane-electrode model and discuss how the model inputs were obtained. The resulting steady-state, coupled, nonlinear, differential equations were solved using Newman's (1973) algorithm.

Transport in the proton-exchange membrane region

The development of the equations for describing the membrane portion of the fuel-cell electrode model are based on the macrohomogeneous description given by Verbrugge and Hill (1990a). A form of the Nernst-Planck equation that includes convection is used to describe the flux of species in the membrane pore fluid (Nernst, 1888, 1889; Planck, 1890),

$$N_i = -z_i\frac{F}{RT}\mathfrak{D}_i c_i\nabla\Phi - \mathfrak{D}_i\nabla c_i + c_i v, \tag{2}$$

which states that a dissolved species can move by migration, diffusion, and convection. Since the flow of charge is related to the current density in the pores of the membrane,

$$i = F\sum_i z_i N_i, \tag{3}$$

we can write for the electric potential

$$\nabla\Phi = -\frac{i}{\kappa} - \frac{F}{\kappa}\left(\sum_i z_i D_i\nabla c_i\right) + \frac{F}{\kappa}\left(\sum_i z_i c_i\right)v, \tag{4}$$

where the conductivity κ is defined as

$$\kappa = \frac{F^2}{RT} \sum_i z_i^2 \mathfrak{D}_i c_i. \tag{5}$$

The summations are over all mobile species i. The first term on the right side of Eq. 4 can be thought of as an Ohm's law contribution; the second is commonly referred to as the diffusion potential; and the last term represents the effect of the potential gradient on the charged-fluid's velocity.

In the absence of specific adsorption of pore-fluid ions onto the membrane structure, the following electroneutrality expression applies:

$$z_f c_f + \sum_i z_i c_i = 0. \tag{6}$$

The fluid dynamics are described by a form of Schögl's equation of motion; electric potential and pressure gradients generate convection within the pores of the ion-exchange membrane (Schlögl, 1955, 1966; Verbrugge and Hill, 1990a):

$$v = \frac{k_\Phi}{\mu} z_f c_f F \nabla \Phi - \frac{k_P}{\mu} \nabla p. \tag{7}$$

Current conservation, expressed as

$$\nabla \cdot \boldsymbol{i} = 0, \tag{8}$$

follows from mass continuity. Along with the steady-state material balance expression,

$$\nabla \cdot N_i = 0, \tag{9}$$

the above equations provide a consistent description of transport in an ion-exchange membrane. The equation of continuity for incompressible fluid flow

$$\nabla \cdot v = 0 \tag{10}$$

can be applied to eliminate the velocity variable from the set of equations.

For the membrane of a polymer-electrolyte fuel cell, the only mobile ions in the membrane pore fluid are hydrogen ions; hence, Eq. 6 can be written as

$$-z_f c_f = c_{H^+}. \tag{11}$$

That is, the hydrogen-ion concentration in the membrane pore fluid can be considered constant, and diffusion is not a mode of proton transport. This equation can thus be taken as the species material balance, and Eqs. 4 and 5 become

$$\nabla \Phi = -\frac{i}{\kappa} + \frac{F}{\kappa} c_{H^+} v \tag{12}$$

and

$$\kappa = \frac{F^2}{RT} \mathfrak{D}_{H^+} c_{H^+}, \tag{13}$$

respectively. The continuity equation for dissolved-oxygen species results from application of Eqs. 2 and 9:

$$\mathfrak{D}_{O_2}^{\text{eff}} \nabla^2 c_{O_2} = v \cdot \nabla c_{O_2}. \tag{14}$$

(Note that the migration term of the Nernst-Planck expression vanishes because oxygen is not charged.) Equations 7, 8, 10, 12 and 14, in one-dimensional form, are applied in the membrane region of the model and are given in the left panels of Table 1. Equations 7, 8, 10, and 12 result in

$$\nabla^2 \Phi = 0 \quad \text{and} \quad \nabla^2 p = 0;$$

so the pressure and potential profiles throughout the membrane region are linear, and the velocity is constant.

Active catalyst layer

The mathematical description of the membrane portion of the active-catalyst-layer region is very similar to the development given in the previous section; the major difference results from current and water conservation equations. The macrohomogeneous approach (Tiedemann and Newman, 1975) is taken in developing equations for describing the active catalyst region of the model. Current in the membrane phase of the catalyst layer can transfer to the electronically-conductive solid portion of the catalyst layer (that is, carbon and catalyst particles). A Butler-Volmer expression (Newman, 1973; Bard and Faulkner, 1980)

$$\nabla \cdot \boldsymbol{i} = j = a i_0 \{ \exp[\alpha_a f(\phi_{\text{solid}} - \phi)] - \exp[-\alpha_c f(\phi_{\text{solid}} - \phi)] \}, \tag{15}$$

with the concentration dependence of the exchange current density given in the bottom, center panel of Table 1, is used to characterize the potential dependence of the rate of Reaction I (per volume basis).

In this region, we apply material balances based on standard porous-electrode theory:

$$\nabla \cdot N_i = -\frac{s_i}{nF} \nabla \cdot \boldsymbol{i}. \tag{16}$$

Liquid water is produced by the electrochemical reaction—for mass continuity we apply

$$\rho \nabla \cdot v_s = -\frac{s_w}{nF} \nabla \cdot \boldsymbol{i}. \tag{17}$$

Equation 12 is applied with an effective membrane conductivity, and Eq. 7 is applied with effective permeabilities. (The effective properties are discussed in the Parameters and Properties section.)

The continuity equation for dissolved-oxygen species results from the application of Eqs. 2, 16 and 17, and contains a generation term both from water production and oxygen depletion:

$$\mathfrak{D}_{O_2}^{\text{eff}} \nabla^2 c_{O_2} = v \cdot \nabla c_{O_2} + \left(\frac{s_{O_2}}{nF} - \frac{s_w}{nF} \frac{c_{O_2}}{\rho} \right) \nabla \cdot \boldsymbol{i}. \tag{18}$$

The movement of electrons in the solid portion of the catalyst layer is governed by Ohm's law

$$\boldsymbol{i}_{\text{solid}} = -\sigma_c^{\text{eff}} \nabla \phi_{\text{solid}}. \tag{19}$$

Electroneutrality, expressed as

$$\nabla \cdot \boldsymbol{i}_{\text{solid}} + \nabla \cdot \boldsymbol{i} = 0, \tag{20}$$

is used to relate the current in the solid carbon-catalyst matrix to the current in the membrane phase of this model region. In the one-dimensional description, this equation gives

$$-I = i_{\text{solid}} + i, \tag{21}$$

where I is the operating current density and is taken to be negative during operation as a cathode in a (galvanic) fuel cell. Equations 7, 12, 15, 17 and 19 (along with Eq. 21) apply in the active catalyst layer. These equations, in one-dimensional form, are given in the middle panels of Table 1.

Transport in the gas-diffuser region

The Stefan-Maxwell equations are the usual starting point for the description of molecular diffusion in multicomponent gas mixtures. For the diffusion of an n-component ideal-gas through a porous medium, these equations take the form (Hirschfelder et al., 1954; Bird et al., 1960):

$$\nabla x_i = \sum_{j=1}^{n} \frac{RT}{pD_{ij}^{\text{eff}}} (x_i N_{j,g} - x_j N_{i,g}) \quad i = 1,2,\ldots,n, \tag{22}$$

where $N_{i,g}$ is the superficial gas-phase flux of species i averaged over a differential volume element, which is small with respect to the overall dimensions of the system, but large with respect to the pore size. The quantity D_{ij}^{eff} is an *effective* binary diffusivity of the pair i-j in the porous medium. The temperature and pressure dependency of this diffusivity is discussed in the Parameters and Properties section.

In the gas pores (wet-proofed pores) of the gas diffuser, we assume that the water vapor is equilibrated with the water in the liquid pores

$$x_w = x_w^{\text{sat}}, \tag{23}$$

which leads to the relation

$$\nabla x_w = 0. \tag{24}$$

Also, we take the volume fraction of gas pores to be uniform and the gas-phase pressure to be uniform throughout the thickness of the diffuser l_g and equal to the chamber pressure p_L. If we assume that the water flowing through the gas diffuser takes up (or gives off) only a negligible amount of dissolved O_2 and N_2 (compared to the relatively large gas-phase concentrations), then the equations of continuity for oxygen and nitrogen gas takes the forms

$$\nabla \cdot N_{O_2,g} = 0 \quad \text{and} \quad \nabla \cdot N_{N_2,g} = 0, \tag{25}$$

respectively. That is, in the steady state, the fluxes of the nitrogen and oxygen gas species in the pores are constant, and there is no net motion of nitrogen because it is considered inert:

$$N_{N_2,g} = 0. \tag{26}$$

In the gas pores of the cathode, oxygen must diffuse through both water vapor and nitrogen gas, and only two of the three Stefan-Maxwell equations for this system need to be considered, since the relation

$$1 = x_w + x_{O_2} + x_{N_2} \tag{27}$$

applies.

Combining Eqs. 24, 25 and 26 with Eq. 22, written for the nitrogen-gas and water-vapor species, one can obtain

$$\frac{p}{RT} \nabla x_{N_2} = \frac{x_{N_2} N_{O_2,g}}{D_{N_2-O_2}^{\text{eff}}} + \frac{x_{N_2} N_{w,g}}{D_{w-N_2}^{\text{eff}}} \tag{28}$$

and

$$\frac{x_w N_{O_2,g} - x_{O_2} N_{w,g}}{D_{w-O_2}^{\text{eff}}} - \frac{x_{N_2} N_{w,g}}{D_{w-N_2}^{\text{eff}}} = 0. \tag{29}$$

Equation 29 can be solved for $N_{w,g}$ in terms of $N_{O_2,g}$ and placed into Eq. 28. It is convenient to define a dimensionless position variable,

$$\xi = (z - l_m - l_c)/l_g, \tag{30}$$

and a dimensionless flux ν,

$$\nu = \frac{N_{O_2,g} RT l_g}{p_L D_{w-N_2}^{\text{eff}}}. \tag{31}$$

The gas-phase oxygen flux is then related to the current

$$\frac{I}{4F} = N_{O_2,g}. \tag{32}$$

The material balance equation in terms of the dimensionless flux ν is

$$\frac{1}{\nu} \frac{dx_{N_2}}{d\xi} = x_{N_2} r_{N_2} + \frac{x_{N_2} x_w^{\text{sat}}}{1 - x_w^{\text{sat}} - x_{N_2} + \dfrac{x_{N_2}}{r_{N_2}}}, \tag{33}$$

where

$$r_w = \frac{D_{w-N_2}^{\text{eff}}}{D_{w-O_2}^{\text{eff}}} \quad \text{and} \quad r_{N_2} = \frac{D_{w-N_2}^{\text{eff}}}{D_{N_2-O_2}^{\text{eff}}}. \tag{34}$$

This equation appears in dimensional form in the right column of Table 1.

Equation 7, with only the pressure gradient term, is used to characterize the water flow since the fluid is not charged in the gas diffuser. An overall water material balance must include

interaction with the gaseous phase:

$$\rho \nabla \cdot v_s = -\nabla \cdot N_{w,g}, \tag{35}$$

where

$$v_s = -\frac{k^d_{P,s}}{\mu} \nabla p, \tag{36}$$

and the water-vapor flux $N_{w,g}$ can be defined in terms of nitrogen composition by Eqs. 27, 29 and 32. Equation 19, with $i_{\text{solid}} = -I$, also applies. The equations, in one-dimensional form, that are applied in the gas-diffuser portion of the model are given in the right column of Table 1.

An analytic solution for the gas-phase composition in the gas diffuser can be obtained; Eq. 33, in one dimension (z), is a first-order, linear, differential equation, which can be solved for an implicit expression for the nitrogen concentration profile:

$$v(\xi - 1) = \ln\left[\left(\frac{r_{N_2}\left(1 - x^{\text{sat}}_w + \frac{x_{N_2}}{r_w} - x^L_{N_2}\right) + x^{\text{sat}}_w}{r_{N_2}\left(1 - x^{\text{sat}}_w + \frac{x_{N_2}}{r_w} - x_{N_2}\right) + x^{\text{sat}}_w}\right)^{r_{N_2}} \left(\frac{x^L_{N_2}}{x_{N_2}}\right)^K\right], \tag{37}$$

where

$$K = r_{N_2} + \frac{x^{\text{sat}}_w}{1 - x^{\text{sat}}_w}. \tag{38}$$

The boundary condition used was at $\xi = 1, x_{N_2} = x^L_{N_2}$. We discuss later the determination of the chamber composition $x^L_{N_2}$. Equation 37, however, is not used in our computer code because it is not explicit in x_{N_2}. (We use Eq. 33 directly.) We discuss later how this analytic solution can be used in limiting-current calculations.

Boundary conditions

At the membrane ($z = 0$), the boundary conditions

$$\phi = 0, \tag{39}$$

$$p = p_0, \tag{40}$$

and

$$c_{O_2} = 0 \tag{41}$$

apply.

At the membrane/catalyst-layer interface ($z = l_m$), the current in the membrane phase is continuous; the relations

$$\left.\frac{d\phi_{\text{solid}}}{dz}\right|_c = 0 \tag{42}$$

and

$$\left.\kappa \frac{d\phi}{dz}\right|_m = \left.\kappa^{\text{eff}} \frac{d\phi}{dz}\right|_c \tag{43}$$

apply. The superficial flux of liquid water is continuous ($v|_m = \epsilon_{m,c} v|_c$),

$$\left.\frac{k^{\text{eff}}_\Phi}{\mu} z_f c_f F \frac{d\phi}{dz}\right|_c - \left.\frac{k^{\text{eff}}_P}{\mu} \frac{dp}{dz}\right|_c = \left.\frac{k_\Phi}{\mu} z_f c_f F \frac{d\phi}{dz}\right|_m - \left.\frac{k_P}{\mu} \frac{dp}{dz}\right|_m, \tag{44}$$

and the flux of dissolved oxygen is continuous through this internal boundary:

$$\left.\mathcal{D}_{O_2} \frac{dc_{O_2}}{dz}\right|_m = \left.\mathcal{D}^{\text{eff}}_{O_2} \frac{dc_{O_2}}{dz}\right|_c. \tag{45}$$

At the catalyst-layer/gas-diffuser interface ($z = l_m + l_c$), the current in the solid phase, ($i - I$), is continuous

$$\left.\sigma^{\text{eff}}_c \frac{d\phi_{\text{solid}}}{dz}\right|_c = \left.\sigma^{\text{eff}}_d \frac{d\phi_{\text{solid}}}{dz}\right|_d, \tag{46}$$

as is the total flux of water ($\rho \epsilon_{m,c} \epsilon_{w,m} v|_c = \rho v_s|_d + N_{w,g}$)

$$\epsilon_{w,m} \left.\frac{k^{\text{eff}}_\Phi}{\mu} z_f c_f F \frac{d\phi}{dz}\right|_c - \epsilon_{w,m} \left.\frac{k^{\text{eff}}_P}{\mu} \frac{dp}{dz}\right|_c = - \left.\frac{k^d_{P,s}}{\mu} \frac{dp}{dz}\right|_d + N_{w,g}. \tag{47}$$

The dissolved-oxygen concentration in the membrane phase of the active catalyst layer is related to the gas-phase composition in the gas diffuser by a Henry's law constant K_{O_2} defined by:

$$c^{\text{sat}}_{O_2} = (1 - x_{N_2} - x^{\text{sat}}_w) \frac{p_L}{K_{O_2}}. \tag{48}$$

At the face of the gas diffuser, which is in contact with the chamber ($z = L = l_m + l_c + l_g$),

$$p = p_L \tag{49}$$

and

$$x_{N_2} = x^L_{N_2}, \tag{50}$$

An expression for $x^L_{N_2}$ in terms of the stoichiometric flow rate ζ can be obtained from an integral material balance on the air chamber. As mentioned earlier, the chamber gases are assumed to be of uniform composition and in equilibrium with liquid water present in the chamber. In this case, the gas composition in the chamber is not dependent on the amount of water vapor that enters the chamber with the reactant gas. The water-vapor content will, however, affect the net amount of liquid water that exits the chamber. We can define the stoichiometric flow ratio of reactant gas ζ as the ratio of the amount of oxygen

added in the reactant feed to the amount that is required by the electrochemical reaction:

$$\zeta = \frac{p_L}{RT}\frac{x^o_{O_2}\vartheta^o}{N_{O_{2,g}}A}, \tag{51}$$

where ϑ is the gas volumetric flow rate. An overall material balance on the oxygen species results in

$$\vartheta^o x^o_{O_2}\frac{p_L}{RT} = \vartheta x^L_{O_2}\frac{p_L}{RT} + N_{O_{2,g}}A, \text{ or}$$

$$\text{in} = \qquad \text{out}. \tag{52}$$

Equations 51 and 52 provide expressions for ϑ^o and ϑ, respectively, which can be substituted into the overall nitrogen material balance on the chamber

$$x^o_{N_2}\vartheta^o = x^L_{N_2}\vartheta \tag{53}$$

to yield

$$x^L_{N_2} = \frac{(1-x^{sat}_w)\dfrac{\zeta}{\zeta-1}\dfrac{x^o_{N_2}}{x^o_{O_2}}}{1+\dfrac{\zeta}{\zeta-1}\dfrac{x^o_{N_2}}{x^o_{O_2}}} \tag{54}$$

For a given value of stoichiometric flow, the composition in the chamber is independent of current density.

Parameters and properties

We compare our model calculations of polarization as a function of operating current density to the experimental results of Ticianelli et al. (1988a,b). To the best of our ability, the model physical parameters for the membrane/electrode system were chosen to correspond to their system. They used humidified air and Prototech-brand electrodes (20 wt. % Pt), onto which they sputtered platinum (50-nm equivalent thickness, total Pt loading of 0.45 mg/cm^2) to obtain superior behavior relative to unsputtered electrodes. Nafion 117 (of E.I. du Pont de Nemours and Company) was used for the membrane in the Prototech electrode design. The base-case operating conditions are given in Table 2. Since Ticianelli et al. report that their membrane penetrates the electrode to an extent of about 10 μm, we realize that the value for the thickness of the active catalyst layer l_c must be in the range $0.05\times10^{-4} < l_c < 10\times10^{-4}$ cm.

Table 2. Physical Parameters for Base-Case Conditions

Quantity	Value for Base-Case Condition
Membrane thickness, l_m	0.023 cm
Gas-diffusion-cathode thickness, l_g	0.026 cm
Active-catalyst-layer thickness, l_c	0.1×10^{-4} cm
Stoichiometric flow, ζ	3
Inlet nitrogen-oxygen mole ratio, $x^o_{N_2}/x^o_{O_2}$	0.79/0.21
Air-side pressure, p_L	5 atm
Membrane-side pressure, p_0	3 atm
Temperature, T	353 K or 80°C
Thermodynamic open-circuit potential, U_{thermo}	1.197 V

The stoichiometric flow rate ζ given in this table does not necessarily correspond to the work of Ticianelli et al., since they did not report their inlet reactant flow rate. The thermodynamic open-circuit potential for the overall reaction

$$O_2 + 2H_2 \rightleftharpoons 2H_2O \qquad \text{(II)}$$

given in Table 2 at base-case conditions was estimated with the relation (Berger, 1968)

$$U_{thermo} = U^o_{thermo} + 2.3\frac{RT}{4F}\log(p^2_{H_2}p_{O_2}). \tag{55}$$

The calculation is made taking the reference electrode operating with pure hydrogen at the membrane-side pressure p_0 and oxygen gas composition in the chamber (i.e., $z=L$). The reference potential at unit pressure in atmospheres is given by (Berger, 1968)

$$U^o_{thermo} = 1.23 - 0.9\times10^{-3}(T-298), \tag{56}$$

where temperature in the above two equations is in kelvins. The partial pressure $p_{O_2} = x_{O_2}p_L$, where $x_{O_2} = 1 - x^{sat}_w - x_{N_2}$. The compositions x^{sat}_w and x_{N_2} are given by Eqs. 1 and 54, respectively.

The remaining model parameters, as well as methods for interpolation and extrapolation of parameters to operating temperature, are discussed in the following two sections. Unless otherwise indicated, these remaining parameters are assumed to be independent of pressure.

Membrane Properties. The model parameters needed to describe the membrane portion of the mathematical model are given in Table 3. The parameters correspond to the properties of Nafion 117 (of E.I. du Pont de Nemours and Company). The estimated membrane conductivity was obtained by applying Eq. 13 with the value of the estimated proton diffusivity that is also given in the Table 3. This value of $\mathfrak{D}_{H^+}$ at 80°C

Table 3. Membrane Properties at 80°C

Quantity	Value at 80°
Estimated proton diffusion coefficient, $\mathfrak{D}_{H^+}$	4.5×10^{-5} cm^2/s
Estimated ionic conductivity, κ	0.17 mho/cm
Ionic conductivity used to fit data, κ	0.07 mho/cm
Fixed charge site concentration,* c_f	1.2×10^{-3} mol/cm^3
Charge of fixed (sulfonate) sites, z_f	-1
Dissolved oxygen diffusivity, $\mathfrak{D}_{O_2}$	1.2×10^{-6} cm^2/s
Electrokinetic permeability,* k_Φ	1.13×10^{-15} cm^2
Hydraulic permeability,** k_P	1.58×10^{-14} cm^2
Pore-fluid (water) viscosity,† μ	3.565×10^{-4} kg/m·s
Pore-fluid (water) density,† ρ	0.054 mol/cm^3
Saturated water vapor pressure, p^{sat}_w	0.467 atm
Henry's law constant for oxygen in membrane, K_{O_2}	2×10^5 atm·cm^3/mol
Volume fraction membrane in active layer, $\epsilon_{m,c}$	0.5
Volume fraction water in membrane,* $\epsilon_{w,m}$	0.28

*Verbrugge and Hill (1990b)
**Fales et al. (1986)
†Weast (1977)

was estimated using the relation $\mathfrak{D}\mu/T=$ constant (Bird et al., 1960); from Verbrugge and Hill (1990b), $\mathfrak{D}_{H^+}=1.4\times10^{-5}$ cm^2/s at 22°C. A value of 0.07 mho/cm, however, allowed for a better fit of the experimental results; both the estimated and fit conductivity values appear to be reasonable based on available membrane transport data. The equation given by Ogumi et al. (1984)

$$\mathfrak{D}_{O_2}=3.1\times10^{-3}\exp\left(-\frac{2{,}768}{T}\right), \tag{57}$$

where T is in kelvins, is used to estimate the value for the diffusion coefficient of dissolved oxygen in the membrane. These authors also offer the oxygen solubility in the membrane at various temperatures, from which we developed the Henry's law expression

$$K_{O_2}=1.33\times10^{6}\exp\left(-\frac{666}{T}\right), \tag{58}$$

where Henry's constant is in units of atm·cm^3/mol and temperature is in Kelvins. For all other parameters, room-temperature values are taken to apply at 80°C.

In the active catalyst region of the mathematical model, the membrane phase is distributed; to reflect this, we use

$$\mathfrak{D}_{O_2}^{\text{eff}}=\epsilon_{m,c}\mathfrak{D}_{O_2},\quad \kappa^{\text{eff}}=\epsilon_{m,c}\kappa,\quad k_{\Phi}^{\text{eff}}=\epsilon_{m,c}k_{\Phi},$$
$$\text{and}\quad k_P^{\text{eff}}=\epsilon_{m,c}k_P. \tag{59}$$

The active catalyst layer is assumed to be thin enough that it is not tortuous and only a porosity correction is necessary.

Electrode Parameters and Properties. The parameters required to describe the gas diffusion electrode (including the active catalyst region and the gas diffuser) are given in Table 4. The conductivity of the electronically-conductive carbon material given in this table is that of graphite carbon (25°C)

Table 4. Electrode Parameters and Properties

Quantity	Value at 80°
Electronic conductivity of solid (C,Pt),* σ	120 mho/cm
Volume fraction electronically conductive solid (C,Pt), ϵ_{solid}	0.3
Gas-pair pressure-diffusivity product, $pD_{O_2-N_2}$	0.279 atm·cm^2/s
Gas-pair pressure-diffusivity product, $pD_{w,-N_2}$	0.387 atm·cm^2/s
Gas-pair pressure-diffusivity product, $pD_{w,-O_2}$	0.370 atm·cm^2/s
Gas-phase volume fraction (wet-proofed pores) ϵ	0.5
Hydraulic permeability (liquid water), $k_{P,s}^{d}$	3.03×10^{-12} cm^2
Number of electrons, n	4
Stoichiometric coefficient for water, s_w	2
Stoichiometric coefficient for O_2, s_{O_2}	-1
Reference exchange current density times area, ai_0^{ref}	5×10^{-4} A/cm^3
Cathodic transfer coefficient, α_c	2
Anodic transfer coefficient, α_a	2
Proton reference concentration, $c_{H^+}^{\text{ref}}=c_f$	1.2×10^{-3} mol/cm^3
Oxygen reference concentration, $c_{O_2}^{\text{ref}}$	4.62×10^{-6} mol/cm^3
O_2 concentration parameter for i_0, γ_{O_2}	1

*Weast (1977)

and is taken to be related to the effective solid-phase conductivity by the Bruggeman-type relation (Meredith and Tobias, 1962)

$$\sigma_c^{\text{eff}}=\sigma_d^{\text{eff}}=\epsilon_{\text{solid}}^{1.5}\sigma \tag{60}$$

Estimates of three gas-pair diffusion coefficients D_{ij}^{eff} are required in the model. The free diffusion coefficients D_{ij} given in Table 4 are estimated with an expression developed from a combination of kinetic theory and corresponding states arguments (Bird et al., 1960):

$$D_{ij}=\frac{C_1T^{C_2}}{p}, \tag{61}$$

where C_2 is a tabulated, empirically-determined constant, and C_1 is a function of the critical properties of the i and j species. Note that the pressure-diffusivity product is only a function of temperature; this diffusivity is virtually independent of composition. We relate the effective diffusion coefficient to the diffusion coefficient in a nonporous system D_{ij} by

$$D_{ij}^{\text{eff}}=D_{ij}\epsilon^{1.5}, \tag{62}$$

where the gas-phase volume fraction ϵ is obtained from the work of Burshtein et al. (1972). As part of this work, we measured experimentally the flow of water through a gas diffusion electrode with a known pressure differential to obtain the estimate of the permeability $k_{P,s}^{d}$ given in Table 4.

Reaction I defines the stoichiometric coefficients and electron number. The product of exchange current density at reference composition and active area in Table 4 was obtained from comparing model calculations to experimental results and is discussed later. The cathodic transfer coefficient was taken from the work of Maoka (1988). The particular value of the anodic transfer coefficient does not significantly affect our model results. The oxygen reference concentration is given by Eq. 48 using the nitrogen composition $x_{N_2}^{L}$.

Results

Figure 2 compares the calculated air-electrode voltage (relative to a hydrogen reference electrode at 3 atm placed at the membrane/reservoir interface, $z=0$) to experimental fuel-cell voltage given by Ticianelli et al. (1988a,b) as a function of current density. Since they report that the hydrogen electrode in their fuel cell performed with negligible overpotentials (for current densities up to 1 A/cm^2), their cell potential data are comparable to our calculated potentials for the membrane /air-electrode model. The model electrode potential in Figure 2 is defined as

$$\text{Electrode Potential}=U_{\text{thermo}}-\eta_{\text{tot}}|_{z=0}, \tag{63}$$

where U_{thermo} is defined by Eq. 55 and η_{tot} is defined by Eq. 64.

Two model parameters were adjusted to obtain the results given in Figure 2: ai_o^{ref} and κ. From 0 to approximately 200 mA/cm^2, the electrochemical-reaction resistance is responsible for most of the polarization, as opposed to potential drop across the membrane. We, therefore, adjusted the parameter

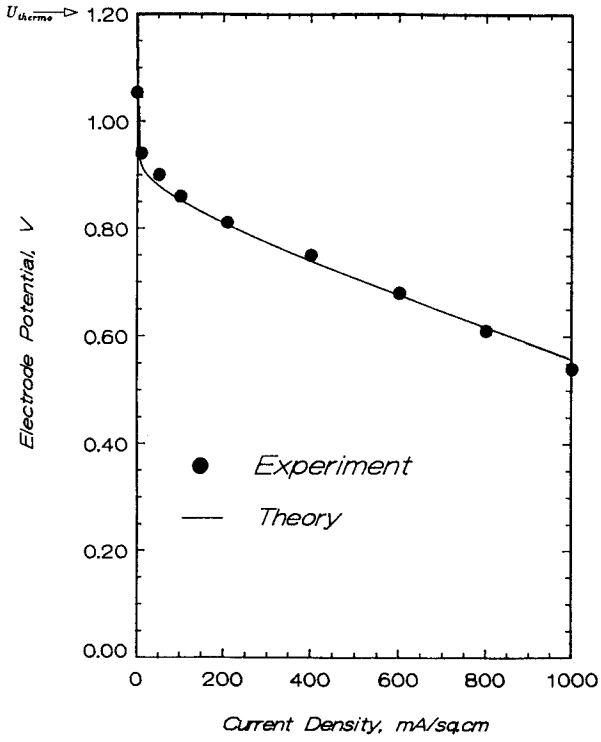

Figure 2. Polarization at base-case conditions (Tables 2, 3 and 4).

The experimental data correspond to the polymer-electrolyte fuel-cell data of Ticianelli et al. (1988a,b), 20 wt. Pt, 50-nm Pt sputter. The solid curve represents our model results for the membrane/air-electrode potential relative to a hydrogen reference electrode.

ai_0^{ref} (see Table 4) to give agreement with the experimental results in this low current density range. For current densities greater than 200 mA/cm^2, the potential drop across the membrane becomes an important source of polarization; we adjusted κ (see Table 3) to give agreement with the experimental results in this high current density range. Thus, at low current densities (< 100 mA/cm^2), the potential drops rapidly due to activation overpotential of the oxygen reduction reaction; and at higher current densities, the potential drops almost linearly

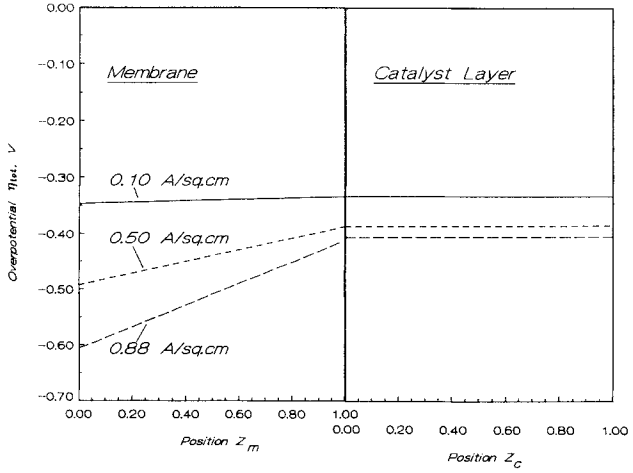

Figure 3. Model results for spatial variation of total overpotential (Eq. 64) through membrane and active catalyst regions for various current densities (base-case conditions).

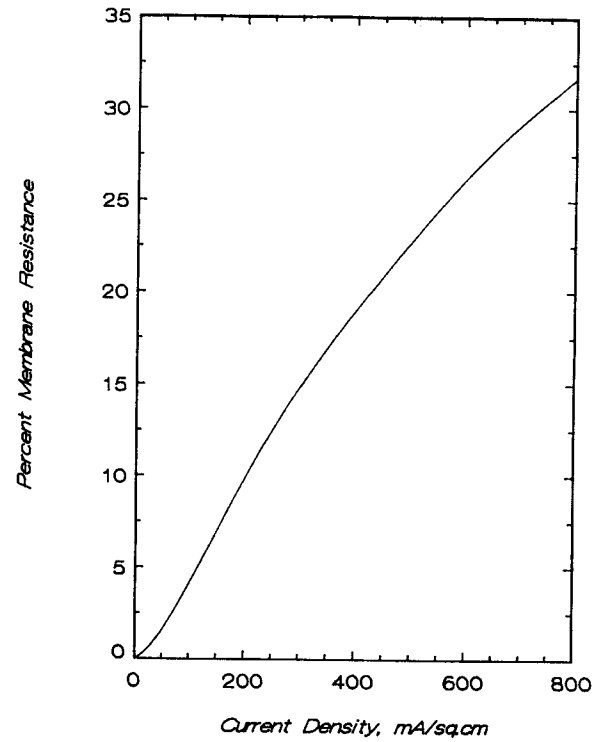

Figure 4. Model results for membrane resistance as a percent of the total resistance vs. cell current density (base-case conditions).

with increasing current density due to the greater influence of potential drop through the membrane, which is illustrated in Figure 3. Figure 3 shows the total overpotential (as measured by an oxygen reference electrode) throughout the membrane and catalyst layer for three current densities. In this figure, the total overpotential is defined as

$$\eta_{tot}(z) = \phi_{solid}|_{z=L} - \phi(z), \tag{64}$$

and the dimensionless distances are defined as

$$Z_m = \frac{z}{l_m}, \quad Z_c = \frac{z - l_m}{l_c}, \quad \text{and} \quad Z_g = \frac{z - l_m - l_c}{l_g}. \tag{65}$$

Figure 3 shows that at 0.1 A/cm^2 operating current density, the membrane does not significantly contribute to the overpotential. At 0.88 A/cm^2, the potential drop through the membrane represents a much more appreciable fraction of the total overpotential. That is, the total overpotential evaluated at $Z_m = 0$ is approximately 0.60 V, of which about 0.41 V is due to activation overpotential and 0.19 V is due to the membrane resistance. For all conditions investigated in this work, the potential drop through the solid phase is negligible (less than 0.001 V).

Figure 4 shows the fraction of the total overpotential, evaluated at the membrane/reservoir interface ($Z_m = 0$), that is due to the membrane resistance as a function of operating current density. Again, we see that resistance through the membrane is only a minor contributor to total overpotential for current densities less than 200 mA/cm^2.

Figure 5 shows the distribution of current density (based on

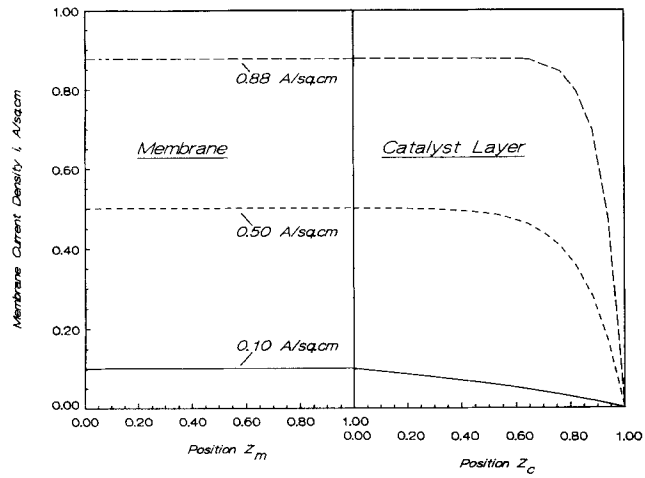

Figure 5. Model results for spatial variation of current density within the membrane phase of both membrane and active catalyst regions for various current densities (base-case conditions).

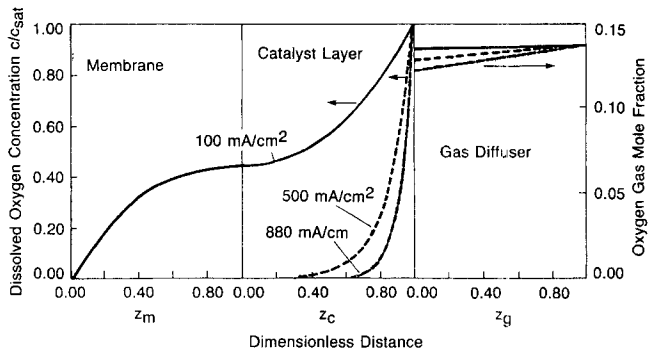

Figure 7. Model results for spatial variation of dissolved-oxygen concentration within membrane and membrane phase of the catalyst layer for various current densities and base-case operating conditions.

The far right panel shows the oxygen-gas mole fraction within the gas diffuser.

superficial area) within the membrane phase in both the membrane region and catalyst layer. The current density is constant throughout the membrane region. In the catalyst layer region, the membrane phase gradually transfers its current density to the solid, electronically-conductive phase (carbon and platinum) via Reaction I, as indicated by the decrease in i to zero at the active-catalyst/diffuser interface. The amount of catalyst enters into the mathematical model through the electrochemically-active-area parameter a, which is multiplied by the exchange current density i_0^{ref} wherever it appears in the model. An increase in the amount of catalyst, therefore, has the same effect as an increase in the exchange current density—a decrease in reaction overpotential. As one would expect, large values of a are desirable: that is, catalyst should be distributed to give a large surface area. The reaction rate j is related to the divergence of the membrane current density as given by Eq. 15. It corresponds to the coulombs of electrons (Reaction I) transferred from the membrane to the solid phase per unit volume of the active catalyst region.

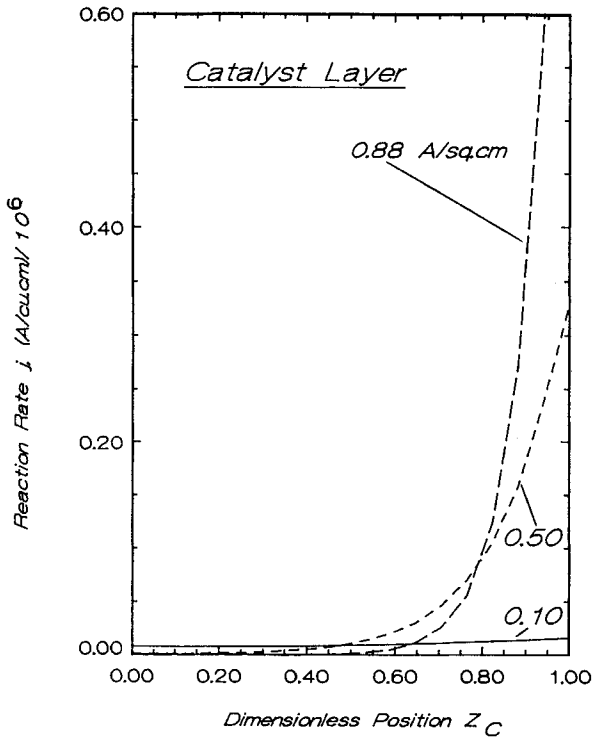

Figure 6. Model results for spatial variation of reaction rate j throughout active catalyst layer for various current densities (base-case conditions).

Figure 6 gives reaction-rate distributions throughout the catalyst layer for three operating current densities. For current densities less than 0.1 A/cm^2, the reaction rate is distributed almost uniformly throughout the catalyst layer: that is, at lower current density, the catalyst can be utilized most effectively because the reaction occurs more uniformly throughout the active layer than at high current density. At higher current densities, the distribution corresponds more to the dissolved-oxygen concentration in the membrane portion of the catalyst layer because the exchange current density is presumed to follow the relationship given in the bottom, center panel of Table 1.

Figure 7 shows dissolved-oxygen concentration profiles in the membrane and the membrane portion of the catalyst layer, as well as the gas-phase oxygen composition in the gas diffuser. Similar to the reaction-rate distribution, the dissolved-oxygen concentration in the catalyst layer is nearly uniform for the low current density result shown. At higher current densities, the back portion of the catalyst layer (near $z_c = 0$) is depleted of dissolved oxygen, because the oxygen cannot diffuse fast enough to replenish what is consumed via Reaction I. It should be mentioned that, even though the oxygen concentration is vanishingly small in the back portion of the catalyst layer for $I > 0.5$ A/cm^2, *limiting current* conditions are not reached until c_{O_2} tends to zero throughout the whole catalyst layer. If O_2 equilibrium exists at the catalyst-layer/diffuser interface ($Z_g = 0$ and $Z_c = 1$), then limiting current conditions will occur when the gas-phase composition of oxygen at $Z_g = 0$ tends to zero. (This is discussed in greater detail in the next paragraph.) Therefore, at high current densities, the model results of Figures 6 and 7 suggest that only a very small portion of the active catalyst layer can be utilized due to dissolved-oxygen transport limitations. These results suggest that, in practice, platinum

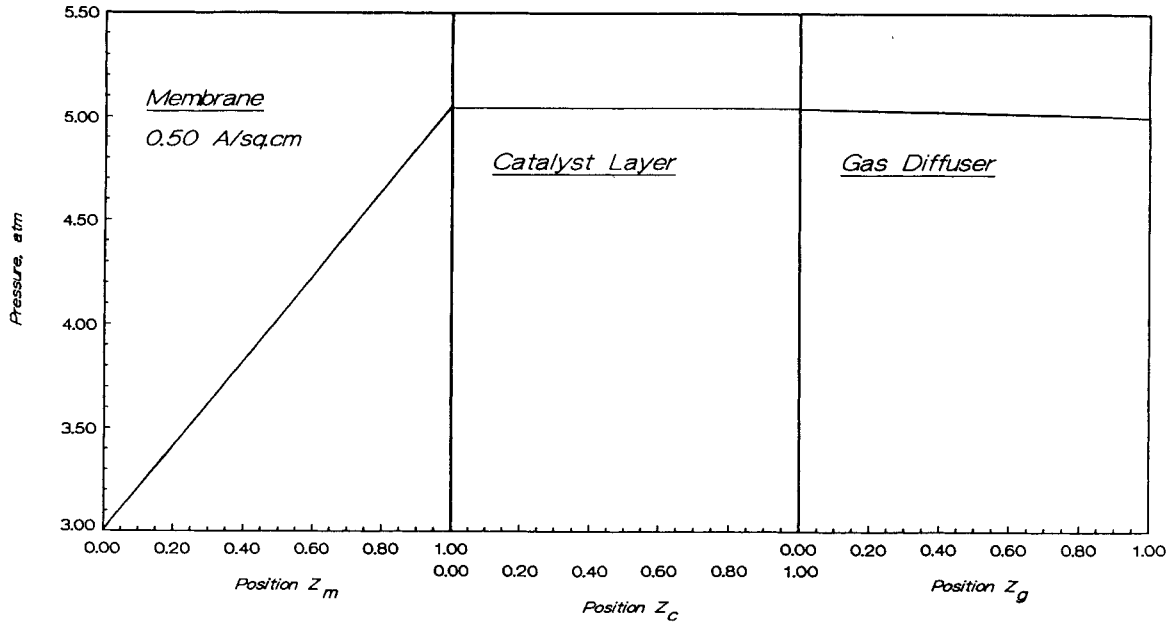

Figure 8. Model results for spatial variation of pressure within hydrophilic portions of the membrane, catalyst-layer, and gas-diffuser regions for various current densities (base-case conditions).

should be localized at the depth that the membrane penetrates the gas diffusion electrode ($z = l_c + l_m$) as opposed to the surface ($z = l_m$). For example, if a given method of affixing the membrane to the gas diffusion electrode allows the membrane to penetrate 5 μm into the electrode, then catalyst should be localized at the depth of 5 μm. The methods of catalyst impregnation, as well as ways to attach the membrane to the electrode, must be optimized to approach this situation as closely as possible.

The composition profiles given for the gas diffuser portion of the model show that oxygen gas transport limitations are essentially nonexistent at these current densities. Equation 37 provides an estimate of the limiting current density based on O_2 gas transport. The application of Eq. 37 at the catalyst-layer/gas-diffuser interface ($\xi = 0$) with $x_{O_2} = 0$ and $x^L_{N_2} = 0.77$ from Eq. 54 gives the dimensionless limiting current $\nu_{lim} = 0.11$ for the results of the base-case operating conditions. The diffusion-limited current density of $I_{lim,O_2} = 7.4$ A/cm^2 can be estimated with ν_{lim}, and Eqs. 32 and 31. This current density may appear high; mass transport limitations are believed to be important at much lower operating current densities (Ticianelli et al., 1988a,b). It must be realized that in our calculation of I_{lim,O_2} from ν using Eq. 31, we have assumed that the volume fraction of gas pores ϵ is 0.5. In reality, ϵ may be much lower because of water blocking the gas pores in near-flooding conditions, and the effective diffusion coefficient $D^{eff}_{w-N_2}$ may tend to very small values (Eq. 59). This result, however, reflects the importance of proper wet proofing in the electrode design—if the pores *could* be kept free of water, then oxygen-gas transport limitations would be seen only at relatively high operating current densities. Conversely, if an estimate of the actual limiting current density were available from experimental results, then an estimate of fraction of open pores ϵ at limiting current conditions could be made.

Figure 8 shows the pressure profile within the hydrophilic regions of the membrane-electrode system; the model results indicate that it is essentially independent of operating current density below 1,000 mA/cm^2. The pressure drop occurs primarily through the membrane because of the membrane's relatively low permeability. The imposed pressure differential of 2 atm acts to reduce the electroosmotic-velocity effect.

Figure 9 shows water velocity profiles at three different current densities. At an operating current density of 125 mA/cm^2, the pressure gradient term on the right side of Eq. 7 dominates, because potential drop through the membrane is not important at the lower current density. Since the pressure forces dominate the water transport, water flow is toward the membrane (from right to left in Figure 1, or water flows out at $z = 0$). At the higher current density of 175 mA/cm^2, the potential gradient term in Eq. 7 dominates, and water flow is toward the diffuser (from left to right in Figure 1, or water flows out at $z = L$).

The case also exists at intermediate values of operating current density where the water that is produced within the catalyst layer will flow out both sides of the membrane-electrode system

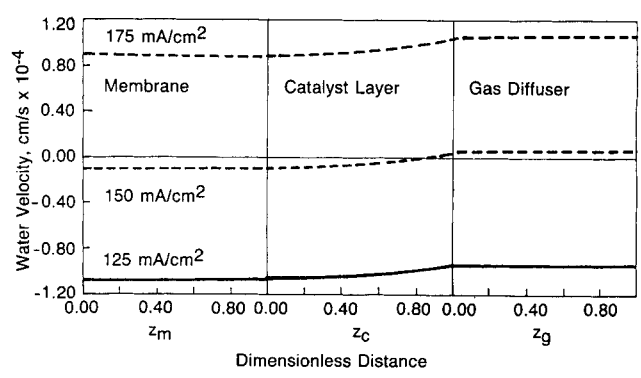

Figure 9. Model results for spatial variation of liquid-water velocity within hydrophilic portion of the membrane, active-catalyst-layer, and gas-diffuser regions (base-case conditions).

as shown for the case of 150 mA/cm^2. This case probably represents the most preferable mechanism of water transport in a polymer-electrode fuel cell, because membrane dehydration will not occur. Unfortunately, our model results suggest that this situation occurs over only a small range of operating current densities—approximately $125 < I < 175$ mA/cm^2 for the values of k_Φ, k_P, and $k^d_{P,s}$ given in Tables 3 and 4. The situation results from a balance between pressure forces and electro-osmotic forces and will maintain the membrane in a fully-saturated state. The situation as depicted for $I > 175$ mA/cm^2 is probably the case for operating conditions of practical polymer-electrolyte fuel cells. A complete model of the polymer-electrolyte fuel cell as well as more experimental verification of the membrane and electrode permeabilities would provide greater insight into this important aspect of cell operation.

It should also be mentioned that at low operating current densities (for our base case, $I < 125$ mA/cm^2), there may be no advantage to operating with a pressure differential. In this situation, more water than is produced by the electrochemical reaction is pushed from right to left in Figure 1, so membrane dehydration could occur at the cathode side of the membrane. This may not be as detrimental to fuel-cell performance as the situation with flow from left to right, because it occurs at low operating current densities when membrane resistance is already relatively insignificant.

The effect of PTFE loading in the gas diffuser—the success of the electrode's wet-proofing agents—manifests itself through two parameters $k^d_{P,s}$ and ϵ. An increase in PTFE loading will increase the volume fraction of wet-proofed pores and also decrease the permeability $k^d_{P,s}$. This will also serve to keep the volume fraction of gas pores ϵ high, and reduce gas-transport limitations and water flow out the diffuser.

Conclusions

We have developed a macrohomogeneous description of a membrane/air-fed electrode, and its predicted polarization behavior compares well with experimental results. The model gives the relative importance of the various resistances that can limit fuel-cell performance. Resistance due to the oxygen reduction reaction appears to be important during all practical operating current densities. If the membrane maintains full saturation, its resistance becomes significant at current densities greater than approximately 200 mA/cm^2. Calculations of reaction rate distributions suggest optimal localization of catalyst. For low current densities, the reaction rate distribution is nearly uniform; at higher current densities, however, the reaction distribution is highly nonuniform, with most of the reaction located in the portion of the catalyst layer near the oxygen-rich catalyst-layer/gas-diffuser interface.

These results indicate that concentrating catalyst near the catalyst-layer/gas-diffuser interface should prove cost-effective. Obviously, any catalyst outside the region of electrode-membrane overlap (that is, the active catalyst layer of this work) is wasted. A novel feature of this work is that we are able to simulate water transport that is driven by pressure and electric-potential forces; water transport is known to play a key role in the operation of polymer-electrolyte cells. Under typical operating conditions, the cathode chamber is pressurized above that of the anode. Our results show that at low current densities, water is forced out from the cathode of the membrane side of the electrode by the pressure differential; in contrast, at high current densities, electro-osmotic forces overcome pressure forces, and water is forced out of the gas-chamber side of the electrode. At intermediate current densities, the pressure and electro-osmotic forces balance and water flows out both sides of the electrode.

Notation

a = effective catalyst area per unit volume cm^2/cm^3
A = superficial electrode area (perpendicular to the z direction), cm^2
c = concentration, mol/cm^3
C_1 = constant in diffusivity expression, Eq. 61
C_2 = constant in diffusivity expression, Eq. 61
$D_{i,j}$ = diffusivity of the gas pair i-j in a mixture, cm^2/s
$\mathfrak{D}$ = diffusion coefficient of a membrane species, cm^2/s
f = quantity defined as $F/(RT)$, V^{-1}
F = Faraday's constant, 96,487 C/equivalent
i_0 = exchange current density, A/cm^2
i = current density, A/cm^2
I = cell current density based on superficial electrode area, A/cm^2
I_{lim,O_2} = diffusion-limiting current density for oxygen, A/cm^2
j = transfer current density, A/cm^3
k_P = membrane hydraulic permeability, cm^2
$k^d_{P,s}$ = hydraulic permeability of diffuser (Eq. 36), cm^2
k_Φ = electrokinetic permeability, cm^2
K = constant defined by Eq. 38
K_{O_2} = Henry's constant for oxygen, atm·cm^3/mol
l_c = thickness of the active catalyst region, cm
l_g = thickness of the gas diffuser, cm
l_m = thickness of the membrane region, cm
n = number of electrons participating in a reaction
n = number of components in a gas mixture
N_i = superficial flux of species i, mol/cm^2·s
p = pressure, atm
p_i = partial pressure of species i, $x_i p$, atm
r = diffusivity ratio, Eq. 34
R = universal gas constant, 8.3143 J/mol·K
s = stoichiometric coefficient
T = absolute temperature, K
U_{thermo} = thermodynamic, open-circuit potential, V
x_i = gas-phase mole fraction of species i
v = pore-water velocity in membrane, cm/s
v_s = superficial water velocity, cm/s
z = distance, cm
z_i = charge number of species i ($i \neq f$)
Z = dimensionless distance

Greek letters

α_a, α_c = anodic and cathodic transfer coefficients, respectively
ϵ = volume fraction of gaseous phase
$\epsilon_{m,c}$ = volume fraction of membrane in catalyst layer
ϵ_{solid} = volume fraction of solid phase in electrode
$\epsilon_{w,m}$ = volume fraction of liquid in membrane
ζ = stoichiometric flow ratio, Eq. 51
ϑ = volumetric flow rate, cm^3/s
κ = membrane conductivity, mho/cm
μ = pore-fluid viscosity, g/cm·s
ν = dimensionless flux defined by Eq. 31
ρ = density of liquid water in the membrane, mol/cm^3
ξ = dimensionless distance
σ = conductivity of the electronically-conductive phase, mho/cm
ϕ = potential, V

Subscripts

c = catalyst layer region
d = gas diffuser
f = membrane species (the fixed charge site species)
g = gas phase

i = mobile species i ($i \neq f$)
L = at the chamber/gas-diffuser interface
lim = limiting current conditions
m = membrane region
solid = in the solid electronically-conductive phase
w = water
0 = at the membrane/reservoir interface

Superscripts

eff = effective, accounting for porous medium
L = at the chamber/gas-diffuser interface
o = inlet to gas chamber
ref = at a reference composition
sat = saturated condition

Literature Cited

Bard, A. J., and L. R. Faulkner, *Electrochemical Methods*, Wiley, New York (1980).

Björnbom, P., "Influence of Diffusion Resistances on Gas Diffusion Electrodes," *J. Electrochem. Soc.*, **133**, 1874 (1986).

Björnbom, P., "Modelling of a Double-Layered PTFE-Bonded Oxygen Electrode," *Electrochim. Acta*, **32**, 115 (1987).

Bird, R. B., W. E. Stewart, and E. N. Lightfoot, *Transport Phenomena*, Wiley, New York, (1960).

Berger, C., ed., *Handbook of Fuel Cell Technology*, Prentice-Hall, Englewood Cliffs, NJ (1968).

Bernardi, D. M., "Water-Balance Calculations for Solid-Polymer-Electrolyte Fuel Cells," *J. Electrochem. Soc.*, **137**, 3344 (1990).

Burshtein, R. Kh., A. V. Dribinskii, M. R. Tarasevich, Yu. A. Chizmadzhev, and Yu. G. Chirkov, "Mechanism of Current Generation of Water-Repellent Gaseous Diffusion Electrodes: I.," *Soviet Electrochemistry*, **7**, 1762 (1971); translated from *Élektrokhimiya*, **7**, 1826 (1971).

Burshtein, R. Kh., A. V. Dribinskii, M. R. Tarasevich, Yu. A. Chizmadzhev, and Yu. G. Chirkov, "Mechanism of Current Generation in Hydrophobized Gas Diffusion Electrodes: II. Dependence of the Electrochemical Activity on the Hydrophobizing Agent in the Active Layer," *Soviet Electrochemistry*, **8**, 195 (1972); translated from *Élektrokhimiya*, **8**, 20 (1972).

Chirkov, Yu. G., "Difference Between Hydrophobized and Hydrophilic Electrodes: III. Cylindrical Gas Pore Model," *Soviet Electrochemistry*, **11**, 36 (1975a); translated from *Élektrokhimiya*, **11**, 43 (1975a).

Chirkov, Yu. G., "Difference Between Hydrophobized and Hydrophilic Electrodes: IV. Forming Physical and Mathematical Models," *Soviet Electrochemistry*, **11**, 41 (1975b); translated from *Élektrokhimiya*, **11**, 50 (1975b).

Giordano, N., E. Passalacqua, V. Alderucci, P. Staiti, L. Pino, H. Mirzaian, E. J. Taylor, and G. Wilemski, "Morphological Characteristics of PTFE Bonded Gas Diffusion Electrodes," *Electrochim. Acta.*, **36**, 1049 (1991).

Fales, J. L., N. E. Vanderborgh, and P. Stroeve, "The Influence of Channel Geometry on Ionic Transport," *Diaphragms, Separators, and Ion-Exchange Membranes*, Vol. 86-13, J. W. Van Zee, R. E. White, K. Kinoshita, and H. S. Burney, eds., The Electrochemical Society, Pennington, NJ (1986).

Fritts, S. D., and R. F. Savinell, "Simulation Studies on the Performance of the Hydrogen Electrode Bonded to Proton Exchange Membranes in the Hydrogen-Bromine Fuel Cell," *J. Power Sources*, **28**, 301 (1989).

Hirschfelder, J. O., C. F. Curtiss, and R. B. Bird, *Molecular Theory of Gases and Liquids*, Chap. 11, Wiley, New York (1954).

Holze, R., and W. Vielstich, "The Kinetics of Oxygen Reduction at Porous Teflon-Bonded Fuel Cell Electrodes," *J. Electrochem. Soc.*, **131**, 2298 (1984).

Jańczuk, B., and T. Bialopiotrowicz, "Adhesion of Air Bubbles to Teflon Surfaces in Water," *J. Colloid. Sci.*, **128**, 1 (1989).

Lindström, O., "That Incredible Fuel Cell," *Chemtech*, p. 490 (Aug., 1988).

Maoka, T., "Electrochemical Reduction of Oxygen on Small Platinum Particles Supported on Carbon in Concentrated Phosphoric Acid: I. The Effects of Platinum Content in the Catalyst Layer and Operating Temperature of the Electrode," *Electrochim. Acta.*, **33**, 371 (1988).

McElroy, J. F., and L. J. Nuttall, "Status of Solid Polymer Electrolyte Fuel Cell Technology and Potential for Transportation Applications," IECEC Meeting, Los Angeles, (Aug. 8–12, 1982).

Meredith, R. E., and C. W. Tobias, "Conduction in Heterogeneous Systems," *Advances in Electrochemistry and Electrochemical Engineering 2*, C. W. Tobias, ed., Interscience Publishers, New York (1962).

Nernst, W., "Zur Kinetik der in Lösung befindlichen Körper: I. Theorie der Diffusion," *Z. Physik Chem.*, **2**, 613 (1888).

Nernst, W., "Die Elektromotorische Wirksamkeit der Jonen: I. Theorie der Diffusion," *Z. Physik Chem.*, **4**, 129 (1889).

Newman, J., *Electrochemical Systems*, Prentice-Hall, Englewood Cliffs, NJ (1973).

Newman, J., "Optimization of Potential and Hydrogen Utilization in an Acid Fuel Cell," *Electrochim. Acta*, **24**, 223 (1979).

Nuttall, L. J., and J. F. McElroy, "Technical and Economic Feasibility of a Solid Polymer Electrolyte Fuel Cell Powerplant for Automotive Applications," SAE IECEC Meeting, Paper No. 830348 (1983).

Ogumi, Z., Z. Takehara, and S. Yoshizawa, "Gas Permeation in SPE Method: I. Oxygen Permeation Through Nafion and NEOSEPTA," *J. Electrochem. Soc.*, **131**, 769 (1984).

Planck, M., "Ueber die Erregung vol Electricität und Wärme in Electrolyten," *Ann. d. Phys. u. Chem.*, **39**, 161 (1890).

Ridge, S. J., R. E. White, Y. Tsau, R. N. Beaver, and G. A. Eisman, "Oxygen Reduction in a Proton Exchange Membrane Test Cell," *J. Electrochem. Soc.*, **136**, 1902 (1989).

Rieke, P. C., and N. E. Vanderborgh, "Thin Film Electrode Arrays for Mapping the Current-Voltage Distributions in Proton-Exchange-Membrane Fuel Cells," *J. Electrochem. Soc.*, **134**, 1099 (1987).

Savinell, R. F., and S. D. Fritts, "Theoretical Performance of a Hydrogen-Bromine Rechargeable SPE Fuel Cell," *J. Power Sources*, **22**, 423 (1988).

Schlögl, R., "Zur Theorie der Anomalen Osmose," *Z. Physik. Chem.*, **3**, 73, Frankfurt, (1955).

Schlögl, R., "Membrane Permeation in Systems Far from Equilibrium," *Ber Bunsenges. Physik. Chem.*, **70**, 400 (1966).

Tiedemann, W., and J. Newman, "Porous-Electrode Theory with Battery Applications," *AIChE J.*, **21**, 25 (1975).

Ticianelli, E. A., C. R. Derouin, A. Redondo, and S. Srinivasan, "Methods to Advance Technology of Proton Exchange Membrane Fuel Cells," *J. Electrochem. Soc.*, **135**, 2209 (1988a).

Ticianelli, E. A., C. R. Derouin, and S. Srinivasan, "Localization of Platinum in Low Catalyst Loading Electrodes to Attain High Power Densities in SPE Fuel Cells," *J. Electroanal. Chem.*, **251**, 275 (1988b).

Van Winkle, J., and W. N. Carson, Jr., "Optimization Calculations for Fuel Cell Systems," *Electrochem. Tech.*, **1**, 18 (1963).

Verbrugge, M. W., and R. F. Hill, "Ion and Solvent Transport in Ion-Exchange Membranes I. A Macrohomogeneous Mathematical Model," *J. Electrochem. Soc.*, **137**, 886 (1990a).

Verbrugge, M. W., and R. F. Hill, "Transport Phenomena in Perfluorosulfonic Acid Membranes During the Passage of Current," *J. Electrochem. Soc.*, **137**, 1131 (1990b).

Watkins, D., K. Dircks, and D. Epp, "Canadian Solid Polymer Fuel Cell Development," *Program and Abstracts from the Fuel Cell Seminar*, Long Beach, CA (Oct., 1988).

Weast, R. C., ed., *Handbook of Chemistry and Physics*, CRC Press, 58th ed., Cleveland, OH, Section f (1977).

Yang, S. C., M. B. Cutlip, and P. Stonehart, "Further Development of an Approximate Model for Mass Transfer with Reaction in Porous Gas-Diffusion Electrodes to Include Substrate Effects," *Electrochim. Acta*, **34**, 703 (1989).

Manuscript received Dec. 26, 1990, and revision received June 17, 1991.